Article

Sublayer-Enhanced Growth of Highly Ordered Mn$_5$Ge$_3$ Thin Film on Si(111)

Ivan Yakovlev [1] , Ivan Tarasov [1,*], Anna Lukyanenko [1,2] , Mikhail Rautskii [1], Leonid Solovyov [3], Alexander Sukhachev [1], Mikhail Volochaev [1,4], Dmitriy Efimov [5], Aleksandr Goikhman [5], Ilya Bondarev [1,4], Sergey Varnakov [1,4] , Sergei Ovchinnikov [1,2] , Nikita Volkov [1] and Anton Tarasov [1,2,*]

1   Kirensky Institute of Physics, Federal Research Center KSC SB RAS, 660036 Krasnoyarsk, Russia
2   Institute of Engineering Physics and Radio Electronics, Siberian Federal University,
    660041 Krasnoyarsk, Russia
3   Institute of Chemistry and Chemical Technology, Federal Research Center KSC SB RAS,
    660036 Krasnoyarsk, Russia
4   Krasnoyarsk Scientific Center, Siberian Branch, Russian Academy of Sciences, 660036 Krasnoyarsk, Russia
5   REC «Functional Nanomaterials», Immanuel Kant Baltic Federal University, 236016 Kaliningrad, Russia
*   Correspondence: ivan.tarasov@uni-due.de (I.T.); taras@iph.krasn.ru (A.T.)

Abstract: Mn$_5$Ge$_3$ epitaxial thin films previously grown mainly on Ge substrate have been synthesized on Si(111) using the co-deposition of Mn and Ge at a temperature of 390 °C. RMS roughness decreases by almost a factor of two in the transition from a completely polycrystalline to a highly ordered growth mode. This mode has been stabilized by changing the ratio of the Mn and Ge evaporation rate from the stoichiometric in the buffer layer. Highly ordered Mn$_5$Ge$_3$ film has two azimuthal crystallite orientations, namely Mn$_5$Ge$_3$ (001) [1-10] and Mn$_5$Ge$_3$ (001) [010] matching Si(111)[-110]. Lattice parameters derived a (7.112(1) Å) and c (5.027(1) Å) are close to the bulk values. Considering all structural data, we proposed a double buffer layer model suggesting that all layers have identical crystal structure with P6$_3$/mcm symmetry similar to Mn$_5$Ge$_3$, but orientation and level of Si concentration are different, which eliminates 8% lattice mismatch between Si and Mn$_5$Ge$_3$ film. Mn$_5$Ge$_3$ film on Si(111) demonstrates no difference in magnetic properties compared to other reported films. T$_C$ is about 300 K, which implies no significant excess of Mn or Si doping. It means that the buffer layer not only serves as a platform for the growth of the relaxed Mn$_5$Ge$_3$ film, but is also a good diffusion barrier.

Keywords: manganese germanide; thin film; MBE; ferromagnetism; sublayer

1. Introduction

Ferromagnetic manganese germanide Mn$_5$Ge$_3$ thin films have been the object of close study for about 20 years [1,2], remaining a promising material for spintronic devices [3,4] since they possess the necessary properties [5]. The Curie temperature T$_C$, which is 296 K for the stoichiometric composition of a bulk crystal [6], can be increased by doping with iron [7], carbon [8], or other dopants [9]. Furthermore, the magnetic properties of such films can be changed via epitaxial stresses [10]. The simplest method for obtaining Mn$_5$Ge$_3$ thin films is solid-phase epitaxy, in which germanium and manganese films are annealed on a substrate [10–12]. There are also several works on the synthesis of epitaxial films using the molecular-beam epitaxy (MBE) method on semiconductor Ge substrates [13–16], and even on GaAs(111) and GaSb(001) [17,18]. However, the successful synthesis of Mn$_5$Ge$_3$ films on Si substrates through direct MBE growth has not been reported, which is most likely due to a rather large lattice mismatch (8%). The solution to this problem will contribute to the creation and study of Mn$_5$Ge$_3$-based magnetic and spintronic devices compatible with silicon CMOS technology. In our work, we demonstrate the successful synthesis of a highly ordered Mn$_5$Ge$_3$ film on a Si(111) substrate using the MBE method, which was implemented by finely tuning the buffer layer.

2. Experimental Details

Mn$_5$Ge$_3$ films were synthesized on p-Si(111) substrate using MBE (base vacuum 6.5×10^{-8} Pa). Si surface was annealed in a vacuum chamber until the 7×7 reconstruction appeared, providing an atomically smooth and clean surface. Then, the silicon substrate was cooled to a temperature of 390 °C, which was kept constant during all experiments. Mn and Ge were co-deposited in certain ratios from Knudsen effusion cells. The process was monitored in situ using reflection high-energy electron diffraction (RHEED). After deposition, the samples were evacuated from the vacuum chamber and thoroughly characterized. X-ray diffraction (XRD) analysis was performed using a PANalytical (Panalytical, Almelo, Netherlands) X'Pert PRO diffractometer equipped with a solid-state detector PIXcel on Cu Ka radiation. Morphology and microstructure of Mn$_5$Ge$_3$ films were studied with atomic force microscopy (AFM) and transmission electron microscopy (TEM) with help of a NanoInk (DPN 5000 device, NanoInk, Skokie, IL, USA) DPN 5000 instrument and Hitachi (Hitachi, Tokyo, Japan) HT-7700 microscope, respectively. To investigate details of the chemical composition of the thin film obtained, Rutherford backscattering spectroscopy (RBS) was used with helium ions, He+, at 1.504 MeV and a scattering angle of 160° relative to the beam's propagation direction. The magnetic properties of the prepared films were examined with the help of a vibrating sample magnetometer (VSM) LakeShore (Lake Shore Cryotronics, Westerville, OH, USA) VSM 8600.

3. Results and Discussion

To determine the conditions for the epitaxial growth of Mn$_5$Ge$_3$ on the Si(111) surface, a series of experiments were performed. Here we show three processes differing in the rate, ratio and time of Mn and Ge deposition during the growth of the buffer layers. These examples demonstrate the effect of buffer layers on the growth processes, structure and morphology of Mn$_5$Ge$_3$ thin films. Schematic diagram of process flow is shown on Figure 1. Sample #1 was synthesized as a single layer at a fixed deposition rate of Mn $V_{Mn} = 0.58$ nm/min and Ge $V_{Ge} = 0.33$ nm/min. During the growth of the first 15 nm, the RHEED pattern transforms from point reflections to streaks and then turns into Debye rings, indicating the formation of a polycrystal (Figure 2a). For sample #2a, one approximately 3 nm thick buffer layer with a low concentration of Mn was grown ($V_{Mn} = 0.2$ nm/min and $V_{Ge} = 0.33$ nm/min).
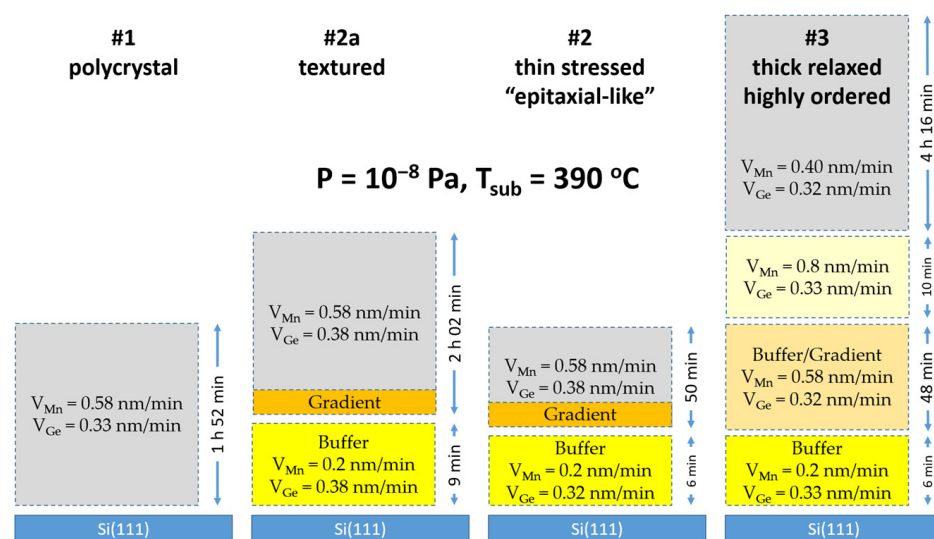

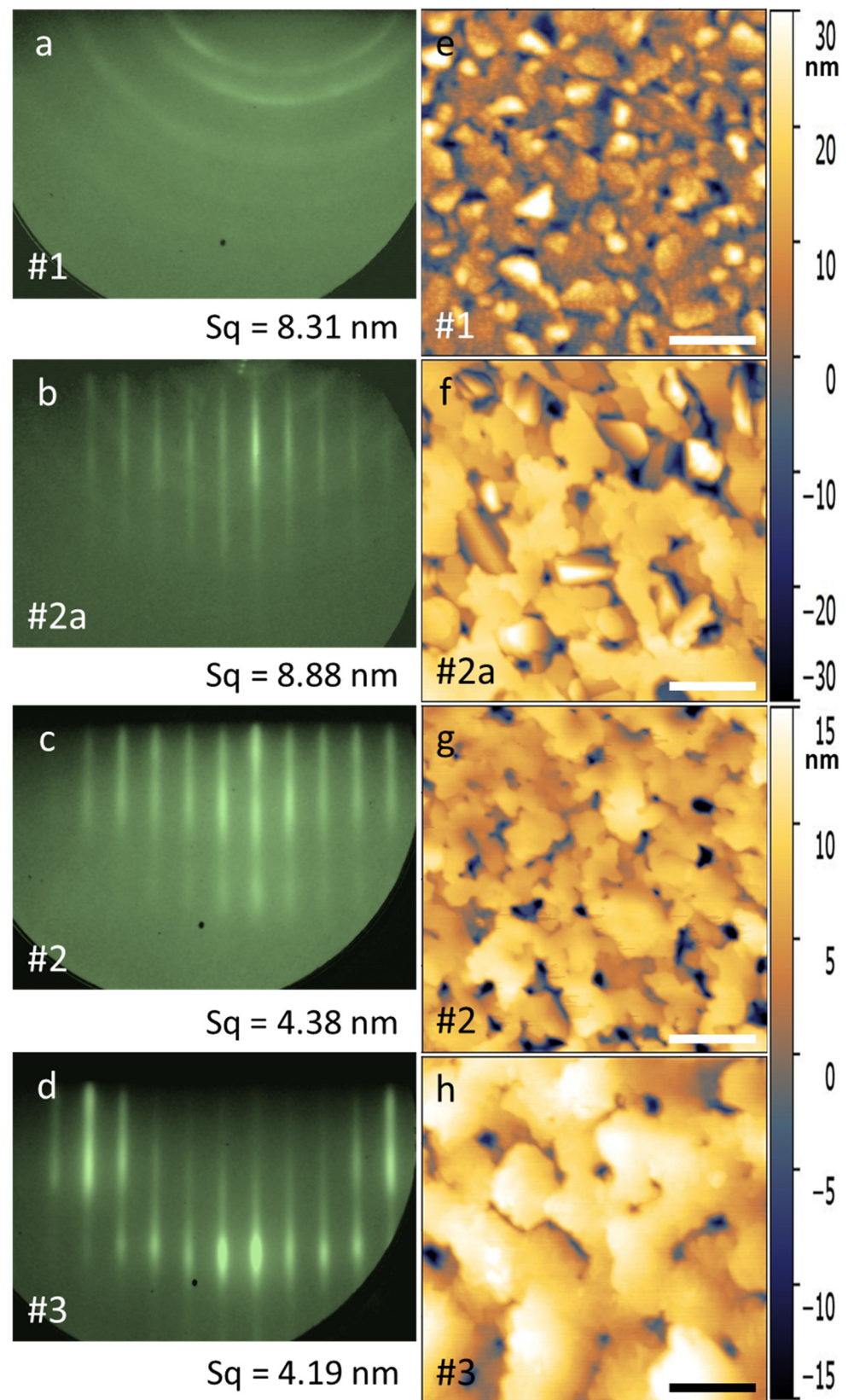**Figure 1.** Diagram of process flow for four different samples.

Figure 2. RHEED pattern and AFM images of the Mn_5Ge_3 thin films on Si(111). RHEED patterns for the samples #1 (**a**), #2a (**b**), #2 (**c**), #3 (**d**) and AFM images for 2 × 2 μm^2 area for the samples #1 (**e**), #2a (**f**), #2 (**g**), #3 (**h**) are shown. The thicknesses of Mn_5Ge_3 films are #1—45 nm, #2a—60 nm, #2—30 nm and #3—150 nm. The length of the scale bar is 500 nm.

Then, within 10 min, the evaporation rate V_{Mn} gradually increased to the stoichiometric value of 0.58 nm/min. At a film thickness of approximately 19 nm, the diffraction pattern contains mainly only lines from a single crystal. This pattern is observed up to 35 nm, after which the rings begin to appear (Figure 2b). This means that with the help of a highly textured buffer layer used, the Mn_5Ge_3 growth can only be stabilized up to a thickness of 35 nm, after which the accumulated stresses in the lattice lead to the formation of crystallites of various orientations. According to this scheme, sample #2 was made with a thickness of about 30 nm. The RHEED pattern for this sample is shown in Figure 2c. To reduce the stresses in the Mn_5Ge_3 film, we added three additional buffer layers. For sample #3, after 3 nm at a rate of $V_{Mn} = 0.2$ nm/min and $V_{Ge} = 0.33$ nm/min, a 25 nm layer followed with a uniform rate increase up to $V_{Mn} = 0.58$ nm/min. Further, V_{Mn} was increased to 0.8 nm/min for 10 min, which corresponds approximately to 10 nm. Thereafter, V_{Mn} decreased to 0.4 nm/min and remained unchanged for 4 h 16 min (approximately 150 nm), during which the RHEED pattern remained as the streaks (Figure 2d). In this case, we were able to stabilize the epitaxy-like growth to relatively large thicknesses.

In addition to RHEED, AFM measurements were performed. As seen in Figure 2, RHEED and AFM correlate well with each other, which is expected since both methods are surface-sensitive. AFM demonstrates a visual image of the surface, which clearly shows the difference between polycrystalline samples #1 and #2a and highly ordered samples #2 and #3. Furthermore, we can compare quantitative parameters such as root-mean-square roughness (Sq) taken over the entire area of the scanning frame (Sq values are marked in Figure 2e–h). Comparing Sq for samples #2a and #3, it can be seen that, upon stabilization of the growth conditions for #3, Sq decreases by almost a factor of two. For two highly ordered samples #2 and #3, the crystallite shape and general surface morphology are similar. However, the size of crystallites for sample #3 is much larger than for sample #2, and one can even talk of the formation of terraces. For a deeper analysis of the crystal structure and composition of the film and buffer layers, an XRD study was carried out. Figure 3a demonstrates XRD profiles for samples #1, #2 and #3.
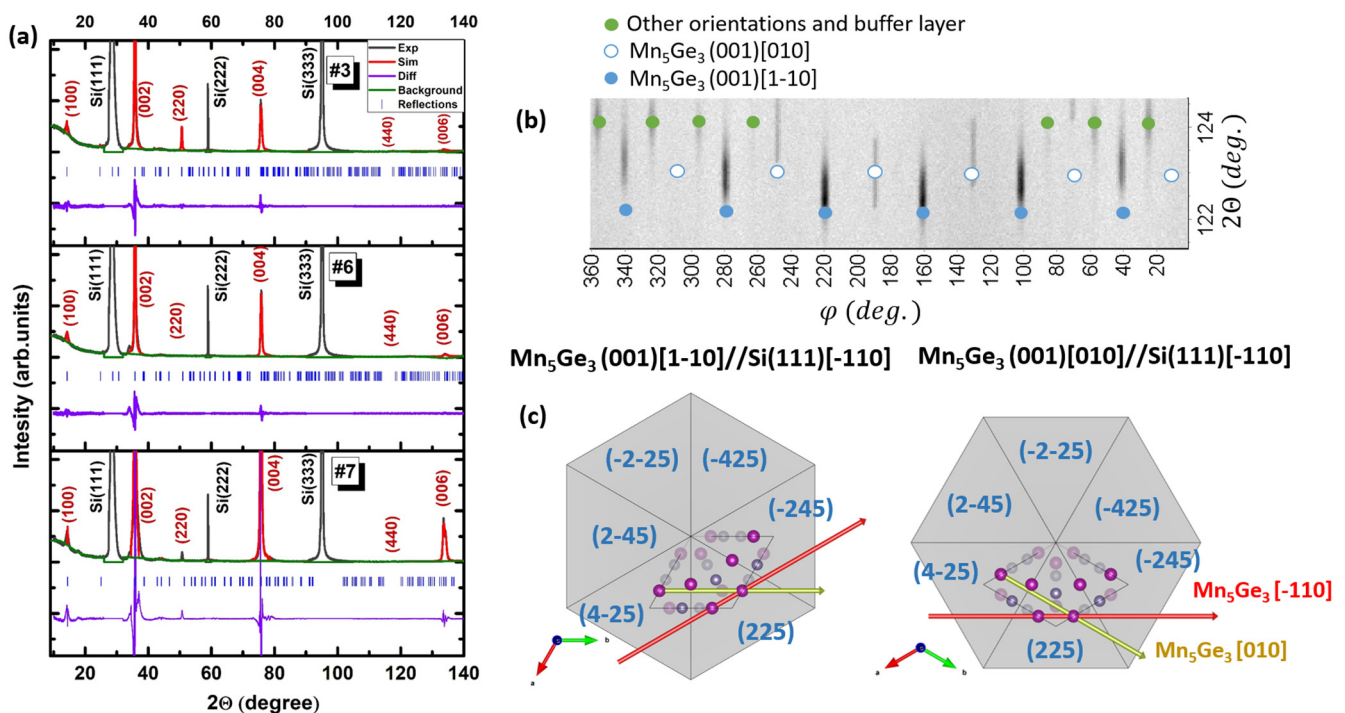

Figure 3. (**a**) XRD profiles for samples #1, #2, #3. (**b**) Phi-scan for sample #3. (**c**) The crystallographic cell of Mn_5Ge_3 at a different orientation parallel to Si(111)[-110].

Similar XRD patterns are observed for all samples. The diffraction peaks are in good agreement with those for the Mn_5Ge_3 with $P6_3/mcm$ space group crystal. The lattice parameters presented in Table 1 were determined via Pawley refinement with the help of GSAS-II software [19]. Silicon diffraction peaks were used for correction of line shift and afterwards excluded from the refinement procedure. Analysis shows that lattice parameters a (7.112(1) Å) and c (5.027(1) Å) are close to the bulk values. It should be noted that the parameters of sample #3 correspond most accurately to the reference lattice parameters. In addition, the intensity of reflection with index (006) at 133.5 degrees on the X-ray pattern increases from sample to sample and reaches a maximum at #3, which indicates good crystalline quality and high texture on the Mn_5Ge_3(001) plane. Consequently, sample #3 was selected for further detailed studies. Figure 3b shows a phi-scan, in which reflections can be interpreted assuming two predominant azimuthal orientations in the (001) plane of Mn_5Ge_3 relative to Si(111), as well as a signal from the buffer layer and other differently orientated crystallites of Mn_5Ge_3, i.e., (100) texture. The formation of a negligible amount of side orientation is explained by a temperature gradient over 40×40 mm substrate. This indicates a high texture on the (001) Mn_5Ge_3 plane and only two crystallite orientations. Figure 3c schematically shows the crystal cells of Mn_5Ge_3 and marks the two orientation relationships derived from the phi-scan.

Table 1. Lattice parameters of Mn_5Ge_3 films along with R-factors obtained by Pawley refinement.

Sample	Lattice Parameters		R_{wp}, %	R_p, %
	a, Å	c, Å		
#1	7.213(1)	5.023(1)	13.10	9.14
#2	7.178(1)	5.020(1)	13.84	8.40
#3	7.112(1)	5.027(1)	12.97	6.15

Sample #3, which has the most complex buffer layer composition and the most ordered structure of the Mn_5Ge_3 film, was further investigated using TEM and electron transmission diffraction (SAED) (Figure 4). In Figure 4a, one can see the columnar structure of the film with relatively large crystallites of 100 nm or more. Figure 4b–e show SAED from film and silicon substrate regions. Pairs of images in Figure 4b–e taken in different directions confirm the presence of two different azimuthal orientations corresponding to the epitaxial relations Mn_5Ge_3 (001)[1-10]//Si(111)[-110] and Mn_5Ge_3 (001)[010]//Si(111)[-110]. At higher magnification (Figure 4f), we can clearly distinguish the buffer layer, as well as see the atomic planes of Si, the buffer layer and Mn_5Ge_3 film. The distances between the Mn_5Ge_3(100) planes increase with the distance from the buffer layer, changing by 3%. Thus, it can be assumed that most (5% of 8%) of the lattice mismatch between Si and Mn_5Ge_3 film is eliminated by the buffer layer.

Summing up the RHEED, XRD and TEM data, several candidates can be suggested, including Mn_3Ge, Mn_5Ge_2 and $Mn_{11}Ge_8$. Taking into account the possible diffusion of silicon from the substrate, $Mn_{10}(SiGe)_3$ and Mn_5Si_2Ge may also be considered. Considering that, in the course of deposition, we tried to reduce the manganese content in the buffer layer, we can assume the formation of $Mn_{11}Ge_8$ or $Mn_5(Si,Ge)_3$ in the buffer layer.

For a more detailed analysis of the composition of the layers, RBS studies were carried out. Experimental and model RBS spectra are presented in Figure 5a. The sum of simulated individual spectra of Ge, Mn and Si has good agreement with experimental data. The calculated depth profile is shown in Figure 5b. On the surface, we can see some oxidation and carbon contamination. Manganese germanide lies deeper with stoichiometry close to Mn_5Ge_3 slightly doped by silicon. Then, the content of manganese and germanium decreases, but the content of silicon increases. This is the transition layer that we are trying to implement in the growing process. However, silicon diffusion additionally occurred in the experiment. It is likely that the area marked with a rectangle in Figure 4f corresponds to a composition of approximately $Mn_5Ge_{1.5}Si_{1.5}$. From here, the decrease in the interplanar

distance indicated in Figure 4f becomes clear. Silicon, having a smaller ionic radius than germanium, reduces the volume of the crystal cell. The lowest layer contains up to 90% silicon. Thus, we can conclude that the buffer layer takes on almost all of the silicon diffusing from the substrate, preventing its incorporation into the main Mn_5Ge_3 layer.
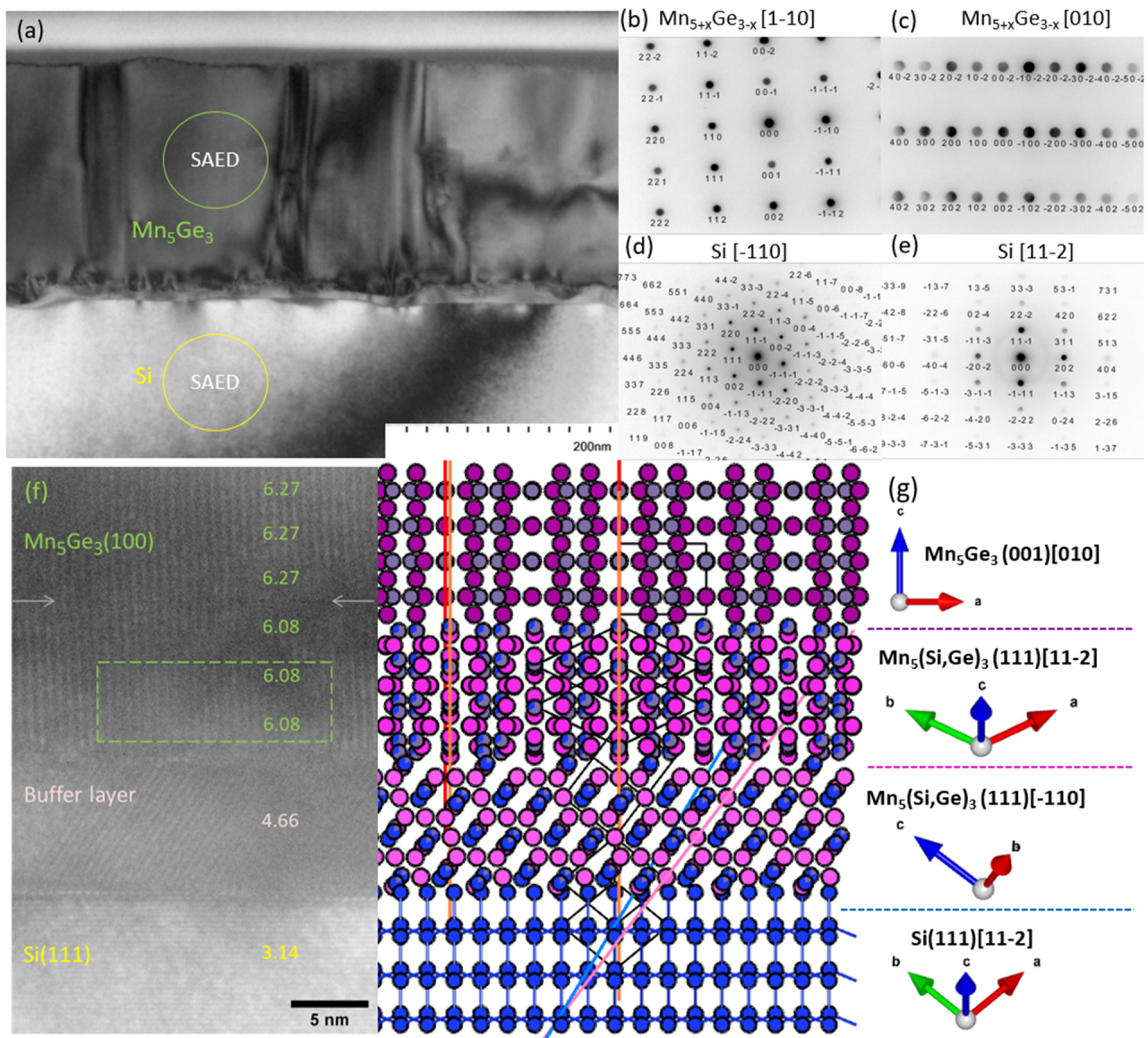

Figure 4. TEM and SAED patterns for sample #3. (**a**) Cross-sectional TEM image of Mn_5Ge_3/Si structure. (**b–e**) Electron diffraction pattern of Mn_5Ge_3 and Si in different crystallographic directions. (**f**) High-resolution TEM near the interface Mn_5Ge_3/Si. Numbers are distances between atomic planes in the arb. units extracted from the image by fast Furrier transform analysis. (**g**) Structural model of the Mn_5Ge_3 growth with two buffer layers of different orientations and levels of Si substitution of Ge sites.

Considering all structural data and assuming RBS layer modelling, we can propose a double buffer layer model as shown in Figure 4g. This model suggests that all layers have identical crystal structures with $P6_3/mcm$ symmetry similar to Mn_5Ge_3, but orientation and level of Si doping are different. Visibly tilted buffer layer (Figure 4f) has $Mn_5(Si,Ge)_3(111)[-110]||Si(111)[11-2]$ orientation. Because of the high Si concentration for this layer, the *c* parameter and the interplanar spacing are closer to Mn_5Si_3 than to Mn_5Ge_3. Next, the intermediate layer is strained $Mn_5(Si,Ge)_3$ with less Si content and $Mn_5(Si,Ge)_3(111)[11-$

2]∥Si(111)[11-2] orientation. The upper film with the biggest volume is relaxed $Mn_5(Ge)_3$ with (001)[010] orientation. Nonetheless, additional azimuthal orientation (001)[1-10] revealed from XRD analysis is presented in the macroscopic film. It should be noted that, estimated from the TEM image (Figure 4f), the angle between the crystal planes of Mn_5Ge_3 and Si do not equal 90 degrees. This indicates an additional tilt of the buffer layer. According to our model (Figure 4g), the buffer layer (100) plane may tend to become parallel to the Si(1-31) plane (blue) for better lattice match. In this case, the whole layer will be slightly tilted, and the subsequent layers too. Similar behavior, in particular, two orientations and a non-90 deg. or 0 deg. angle between the *c*-axis and main substrate direction were observed for Mn_5Ge_3 thin films grown on Ge(001) [19]. Alvídrez-Lechuga et al. [20] name such growth regime epitaxial mosaic-like.
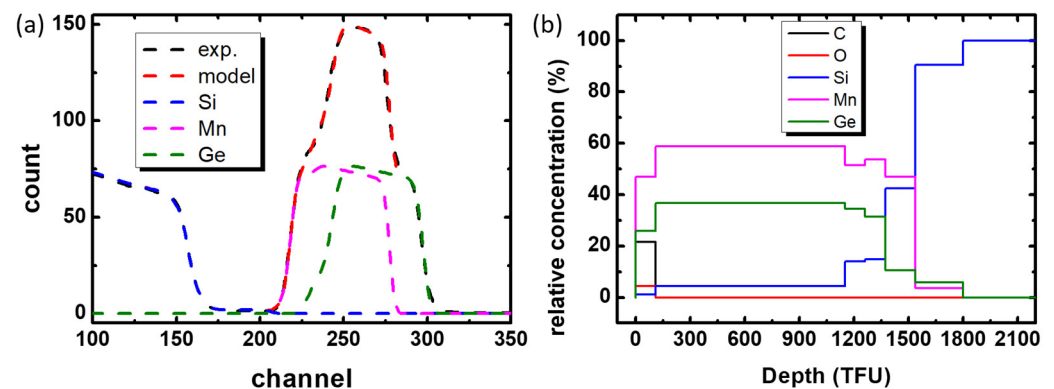

Figure 5. Experimental and model RBS spectra (**a**) and calculated depth profile (**b**) of Mn_5Ge_3/Si sample #3.

To establish the relationship between some physical properties and the structure of the films, the magnetic properties were characterized. From the VSM data, we found that the Curie temperature (T_C) is about 300 K (Figure 6a). For previously synthesized films on Ge substrates, T_C is also about 300 K, which is in good agreement with our samples. For stoichiometric bulk, Mn_5Ge_3 T_C should be close to 296 K [6]. According to [21], an excess of Mn can lead to an increase in the transition temperature, while doping with Si leads to a decrease in T_C [22]. We can, therefore, exclude diffusion of Si from the substrate into the film. According to RBS, a slight excess of Mn and Si doping is possible, which compensates for their effect on T_C and leaves T_C close to the stoichiometric Mn_5Ge_3. It follows that the buffer layer is a good diffusion barrier. Another reason for the deviation of T_C may be stresses in the crystal that affect the magnetic properties. Summing up the diffraction data, we can assume that the main reason for the small increase in T_C is the excess of manganese $Mn_{5+x}Ge_{3-x}$ rather than stresses in the crystal. Epitaxial ordering also does not affect T_C. On Figure 6b, one can see that the extremum of the derivative for all samples corresponds to approximately 300 K. One should note that the width of the ferromagnetic transition is shrinking with consistently increasing the crystal quality of films #1, #2 and #3. Extracted from hysteresis loops (Figure 6c), saturation magnetization M_S is around 1050 emu/cm^3, which is very close to the bulk quoted value of 1070 emu/cm^3 [23] and is similar to reported films' values [15]. Crystal ordering strongly affects magnetic anisotropy, which can be clearly seen from the sharp kink for #3 on Figure 6c.
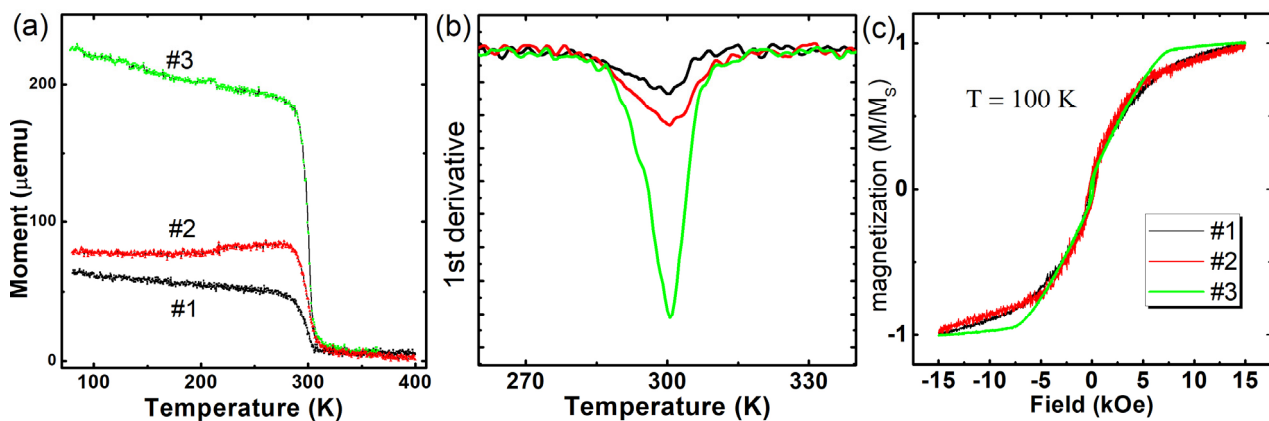
Figure 6. (**a**) Non-normalized magnetization temperature dependencies. (**b**) First derivative of magnetization temperature dependencies. (**c**) Normalized hysteresis loops measured at 100 K for Mn_5Ge_3 samples #1, #2 and #3.

4. Conclusions

The synthesis of Mn_5Ge_3 thin films on Si(111) substrates was performed with varying the rate and time of Mn and Ge deposition at the stages of initial growth. Subsequent gradual decrease and increase in the Mn flux and then return to a stoichiometric ratio of 5:3 make it possible to grow a relaxed highly ordered Mn_5Ge_3 layer with 100% texture on the (001) Mn_5Ge_3 plane. Most (5% out of 8%) of the lattice mismatch between Si and Mn_5Ge_3 film is eliminated by the buffer layer. Considering all structural data, we proposed a double buffer layer model suggesting that all layers have an identical crystal structure and symmetry similar to Mn_5Ge_3, but orientation and level of Si concentration are different. Analysis of XRD and SAED data shows the presence of two different azimuthal orientations corresponding to the epitaxial relations Mn_5Ge_3 (001)[1-10]//Si(111)[-110] and Mn_5Ge_3 (001)[010]//Si(111)[-110]. Examination of the magnetic properties has revealed that the Curie temperature, T_C is about 300 K, which is close to the bulk value (296 K) and coincides with one of the other reported values for films synthesized on different substrates. Furthermore, the elemental composition of the film probed by RBS allowed us to conclude that the buffer layer takes on almost all the silicon diffusing from the substrate, preventing its incorporation into the main Mn_5Ge_3 layer, which is in good agreement with the magnetic properties. We believe that full epitaxial growth can be realized by developing a buffer layer approach and careful substrate temperature control. The observed details of the synthesis of highly ordered Mn_5Ge_3 film can be useful for the growth technology of ferromagnetic epitaxial films on Si(111) substrates and can expand the number of applicable materials in silicon spintronics.

Conflicts of Interest: The authors declare no conflict of interest.

References

1. Zeng, C.; Erwin, S.C.; Feldman, L.C.; Li, A.P.; Jin, R.; Song, Y.; Thompson, J.R.; Weitering, H.H. Epitaxial ferromagnetic Mn_5Ge_3 on Ge(111). *Appl. Phys. Lett.* **2003**, *83*, 5002–5004. [CrossRef]
2. Panguluri, R.P.; Zeng, C.; Weitering, H.H.; Sullivan, J.M.; Erwin, S.C.; Nadgorny, B. Spin polarization and electronic structure of ferromagnetic Mn_5Ge_3 epilayers. *Phys. Stat. Sol. (B)* **2005**, *242*, R67–R69. [CrossRef]
3. Spiesser, A.; Saito, H.; Jansen, R.; Yuasa, S.; Ando, K. Large spin accumulation voltages in epitaxial Mn_5Ge_3 contacts on Ge without an oxide tunnel barrier. *Phys. Rev. B.* **2014**, *90*, 205213. [CrossRef]
4. Fischer, I.A.; Chang, L.T.; Sürgers, C.; Rolseth, E.; Reiter, S.; Stefanov, S.; Chiussi, S.; Tang, J.; Wang, K.L.; Schulze, J. Hanle-effect measurements of spin injection from $Mn_5Ge_3C_{0.8}/Al_2O_3$-contacts into degenerately doped Ge channels on Si. *Appl. Phys. Lett.* **2014**, *105*, 222408. [CrossRef]
5. Bechler, S.; Kern, M.; Funk, H.S.; Colston, G.; Fischer, I.A.; Weißhaupt, D.; Myronov, M.; van Slageren, J.; Schulze, J. Formation of Mn_5Ge_3 by thermal annealing of evaporated Mn on doped Ge on Si (111). *Semicond. Sci. Technol.* **2018**, *33*, 095008. [CrossRef]
6. Maraytta, N.; Voigt, J.; Salazar Mejía, C.; Friese, K.; Skourski, Y.; Perßon, J.; Salman, S.M. and Brückel, Anisotropy of the magnetocaloric effect: Example of Mn5Ge3. *J. Appl. Phys.* **2020**, *242*, 103903. [CrossRef]
7. Austin, A.E. Magnetic Properties of Fe_5Ge_3–Mn_5Ge_3 Solid Solutions. *J. Appl. Phys.* **1969**, *40*, 1381–1382. [CrossRef]
8. Le Thanh, V.; Spiesser, A.; Dau, M.T.; Olive-Mendez, S.F.; Michez, L.A.; Petit, M. Epitaxial growth and magnetic properties of Mn_5Ge_3/Ge and $Mn_5Ge_3C_x/Ge$ heterostructures for spintronic applications. *Adv. Nat. Sci. Nanosci. Nanotechnol.* **2013**, *4*, 043002. [CrossRef]
9. Myagkov, V.; Matsynin, A.; Bykova, L.; Zhigalov, V.; Mikhlin, Y.; Volochayev, M.; Velikanov, D.; Aleksandrovsky, A.; Bondarenko, G. Solid-state synthesis and characterization of ferromagnetic Mn_5Ge_3 nanoclusters in GeO/Mn thin films. *J. Alloys Compd.* **2019**, *782*, 632–640. [CrossRef]
10. Xie, Y.; Yuan, Y.; Birowska, M.; Zhang, C.; Cao, L.; Wang, M.; Grenzer, J.; Kriegner, D.; Doležal, P.; Zeng, Y.J.; et al. Strain-induced switching between noncollinear and collinear spin configuration in magnetic Mn_5Ge_3 films. *Phys. Rev. B.* **2021**, *104*, 064416. [CrossRef]
11. Yasasun, B.T.; Önel, A.C.; Aykac, I.G.; Gulgun, M.A.; Arslan, L.C. Effect of Ge layer thickness on the formation of Mn5Ge3 thin film on Ge/Si (1 1 1). *J. Magn. Magn. Mater.* **2018**, *473*, 348–354. [CrossRef]
12. Alvídrez-Lechuga, A.; Antón, R.L.; Gutiérrez-Pérez, R.M.; Fuentes-Montero, M.E.; Espinosa-Magaña, F.; Holguín-Momaca, J.T.; Andrés, J.P.; Olive-Méndez, S.F. Strong magnetization and anisotropy of Mn5Ge3 thin films on Ge (001). *J. Phys. Condens. Matter* **2021**, *33*, 225802. [CrossRef]
13. Olive-Mendez, S.; Spiesser, A.; Michez, L.A.; Le Thanh, V.; Glachant, A.; Derrien, J.; Devillers, T.; Barski, A.; Jamet, M. Epitaxial growth of Mn5Ge3/Ge (111) heterostructures for spin injection. *Thin Solid Film.* **2008**, *517*, 191–196. [CrossRef]
14. Spiesser, A.; Slipukhina, I.; Dau, M.T.; Arras, E.; Le Thanh, V.; Michez, L.; Pochet, P.; Saito, H.; Yuasa, S.; Jamet, M.; et al. Control of magnetic properties of epitaxial $Mn_5Ge_3C_x$ films induced by carbon doping. *Phys. Rev. B.* **2011**, *84*, 165203. [CrossRef]
15. Spiesser, A.; Virot, F.; Michez, L.A.; Hayn, R.; Bertaina, S.; Favre, L.; Petit, M.; Le Thanh, V. Magnetic anisotropy in epitaxial Mn_5Ge_3 films. *Phys. Rev. B.* **2012**, *86*, 035211. [CrossRef]
16. Petit, M.; Boussadi, A.; Heresanu, V.; Ranguis, A.; Michez, L. Step flow growth of Mn_5Ge_3 films on Ge (111) at room temperature. *Appl. Surf. Sci.* **2019**, *480*, 529–536. [CrossRef]
17. Dung, D.D.; Odkhuu, D.; Thanh Vinh, L.; Cheol Hong, S.; Cho, S. Strain-induced modification in the magnetic properties of Mn_5Ge_3 thin films. *J. Appl. Phys.* **2013**, *114*, 073906. [CrossRef]
18. de Oliveira, R.C.; Demaille, D.; Casaretto, N.; Zheng, Y.; Marangolo, M.; Mosca, D.; Varalda, J. Magnetic and structural properties of $Mn_{5+x}Ge_{3+y}$ thin films as a function of substrate orientation. *J. Magn. Magn. Mater.* **2021**, *539*, 168325. [CrossRef]
19. Toby, B.H.; Von Dreele, R.B. GSAS-II: The genesis of a modern open-source all purpose crystallography software package. *J. Appl. Crystallogr.* **2013**, *46*, 544–549. [CrossRef]
20. Alvídrez-Lechuga, A.; Antón, R.L.; Fuentes-Cobas, L.E.; Holguín-Momaca, J.T.; Solís-Canto, O.; Espinosa-Magaña, F.; Olive-Méndez, S.F. Epitaxial mosaic-like Mn_5Ge_3 thin films on Ge(001) substrates. *J. Alloy. Compd.* **2018**, *762*, 363–369. [CrossRef]
21. Kim, Y.; Kim, E.J.; Choi, K.; Han, W.B.; Kim, H.S.; Yoon, C.S. Magnetocaloric effect of $Mn_{5+x}Ge_{3-x}$ alloys. *J. Alloy. Compd.* **2015**, *620*, 164–167. [CrossRef]
22. Liu, X.B.; Altounian, Z. Magnetocaloric effect in $Mn_5Ge_{3-x}Si_x$ pseudobinary compounds. *J. Appl. Phys.* **2006**, *99*, 08Q101. [CrossRef]
23. Kappel, G.; Fischer, G.; Jaegle, A. On the saturation magnetization of $Mn_5 Ge_3$. *Phys. Lett. A* **1973**, *45*, 267–268. [CrossRef]